The magnetic phase diagram and the effect of pressure on the magnetic properties of the $Y_{1-x}Gd_xMn_2$ intermetallic compounds

1999 J. Phys.: Condens. Matter 11 2937

(http://iopscience.iop.org/0953-8984/11/14/010)

J. Phys.: Condens. Matter **11** (1999) 2937–2953. Printed in the UK PII: S0953-8984(99)99054-9

The magnetic phase diagram and the effect of pressure on the magnetic properties of the $Y_{1-x}Gd_xMn_2$ intermetallic compounds

I S Dubenko†, I Yu Gaidukova‡, Y Hosokoshi§, K Inoue§ and A S Markosyan‡§‖

† Moscow Institute of Radioengineering Electronics and Automation, Prospekt Vernadskogo 54, 117454 Moscow, Russia
‡ Faculty of Physics, M V Lomonosov Moscow State University, 119899 Moscow, Russia
§ Applied Molecular Science, Institute for Molecular Science, Nishigounaka 38, Myodaiji, Okazaki 444-8585, Japan

Received 6 November 1998, in final form 18 February 1999

Abstract. The magnetization up to 50 kOe, the magnetic susceptibility under external pressure up to 5 kbar and the thermal expansion of the cubic Laves phase compounds $Y_{1-x}Gd_xMn_2$ were studied over a wide temperature range. Two well defined concentration regions were isolated in the x–T phase diagram: $0 \leqslant x < 0.2$, in which the antiferromagnetic structure is primarily determined by the d–d interaction (YMn_2-type), and $0.2 < x \leqslant 1$, in which the f–d interaction plays a dominant role ($GdMn_2$-type). It is concluded that both the Gd and the Mn sublattices are ordered in $GdMn_2$ below $T_N = 108$ K, the change in the magnetic characteristics at 40 K being interpreted as an antiferromagnetism–non-collinear ferrimagnetism transition. The intermediate $Y_{0.8}Gd_{0.2}Mn_2$ compound shows a freezing and time-dependent behaviour at low temperatures characteristic of short-range order. The effects can also be induced by external pressure at higher Gd concentrations.

1. Introduction

The phenomenon of magnetic instability, a jump-like change of the magnetic state when the external forces or internal parameters are varied continuously, attracts much attention. For itinerant-electron systems, a number of striking effects accompany this first-order phase transition [1, 2]. The RMn_2 Laves phases have a special place among the rare-earth (RE)–3d intermetallic compounds exhibiting an instability of the 3d magnetism. In this series the Mn sublattice shows intrinsic long-range order when R = Pr, Nd, Sm, Gd, Tb and Y with μ_{Mn} slightly varying from 2.8 to 2.6 μ_B [3, 4]. Magnetic ordering of these compounds occurs through a first-order-type phase transition, which is accompanied by a huge positive volume effect of the order of 10^{-2} [2, 5]. In the compounds with R = Dy, Ho, Er, Tm and Lu, μ_{Mn} is significantly lower, the maximal value 1.4 μ_B being reached in $DyMn_2$ [6]. As no volume expansion is observed in the latter family, no intrinsic long-range order is considered to exist in the Mn sublattice [2, 5].

‖ Author to whom any correspondence should be addressed. Address for correspondence: Applied Molecular Science, Institute for Molecular Science, Nishigounaka 38, Myodaiji, Okazaki 444-8585, Japan; e-mail address: marko@ims.ac.jp.

0953-8984/99/142937+17$19.50

An important feature of the RMn_2 intermetallics is the negative d–d exchange interaction, which is responsible for antiferromagnetic ordering in YMn_2 and stabilizes various non-collinear magnetic structures in the compounds with magnetic REs. It was emphasized that Mn ions form regular tetrahedra, both in hexagonal and cubic Laves phase modifications, which, in view of the negativity of the Mn–Mn exchange interaction, allows one to treat the magnetic structure of the RMn_2 compounds in terms of geometrical frustration [7–9]. Different factors that drive the magnetic instability of Mn magnetism were considered [2, 5].

(a) The concept of the interatomic distance proceeds from the assumption that long-range antiferromagnetic order in RMn_2 is intrinsic and has an abrupt onset when the Mn–Mn nearest-neighbour distance exceeds some critical value r_{cr}. The critical lattice parameter $\approx$7.62 Å, above which the Mn magnetic sublattice is ordered, lies between the values for $TbMn_2$ (7.636 Å) and $DyMn_2$ (7.572 Å) [2, 10]. The existence of long-range order of YMn_2 with non-magnetic yttrium strongly supports this model.

(b) In [5, 11] the importance of the f–d intersublattice exchange interaction in stabilizing the long-range order in the Mn sublattice was revealed. When $H_{mol}^{(Mn)}$ reaches the critical value, the Mn magnetic state changes abruptly, as for the RCo_2 Laves phase compounds with a metamagnetic Co sublattice [1, 12]. According to this mechanism the critical internal field for the onset of long-range order in the Mn sublattice lies between the values of $H_{mol}^{(Mn)}$ of $TbMn_2$ and $DyMn_2$ [2, 13]. This concept can be argued on the basis of the field-induced demagnetization of the Mn sublattice observed in $TbMn_2$ [8, 11, 14]. The effect results from the diminution of the total effective field acting on the Mn sublattice $H_{eff}^{(Mn)} = H_{mol}^{(Mn)} - H_{ext}$ with increasing external magnetic field H_{ext}. As H_{ext} reaches the critical value (8 T at 4.2 K), the magnetization of $TbMn_2$ shows an abrupt increase [11]. This concept is however inconsistent with the existence of long-range order in YMn_2, which prevents one from extending it to the RMn_2 series as a whole.

In fact, the above mechanisms do not conflict with each other. As in the RMn_2 series, the f–d molecular field $H_{mol}^{(Mn)}$ increases in step with the lattice parameter when decreasing the RE atomic number; each factor plays its own role in determining the magnetic behaviour of the Mn sublattice. Nevertheless, the nature of the magnetic instability of the Mn sublattice in these intermetallics remains unclear. Essentially, the models described do not account for the microscopic sources, and only give the parameters that should be used when discussing the magnetic properties of the RMn_2 compounds versus the RE element present.

In [5, 13] an assumption was made that the magnetic order in YMn_2 could be of non-magnetic origin and it was suggested that the intrinsic magnetic ordering arises in the new low-temperature (LT) crystal phase only, while the high-temperature (HT) phase remains paramagnetic. In [14–17] a model was proposed which relates the appearance of the intrinsic magnetic ordering in the Mn sublattice to a diffusionless first-order transformation. According to this model, each Mn atom bears an intrinsic local moment of about 2.7 μ_B in the transformed phase (TP) with a larger lattice parameter, which is stable when the Mn–Mn nearest-neighbour spacing exceeds the critical value. In the non-transformed phase (NTP) with a smaller lattice parameter the Mn subsystem shows a typical itinerant behaviour. When alloyed with a magnetic RE, a paramagnetic moment (up to 1.5 μ_B in $DyMn_2$) can be induced in the Mn subsystem. The volume difference between the two phases reaches several per cent.

As in the case of many other structural phase transitions, the TP and NTP states can coexist over a wide temperature region. The coexistence was observed at low temperatures (in fact, in the ground state) at ambient pressure in YMn_2 [18], $Y_{1-x}Sc_xMn_2$ [19] and $Y_{1-x}La_xMn_2$ [13], and can also be induced by external pressure, as e.g. in the $Tb_{1-x}Y_xMn_2$ and $Dy_{1-x}Y_xMn_2$ systems [17, 20], or by a magnetic field, as was observed for $TbMn_2$ [8]. Many of the unusual

properties that the RMn_2 compounds show, such as a huge volume expansion of about 2–6% at T_N and a huge pressure response of T_N varying from 6 up to 25 K kbar^{-1} [21–24], including the onset of a large tetragonal distortion ($\sim 10^{-3}$) in YMn_2 below T_N [18], can be accounted for by the TP–NTP transformation model.

In the NTP state, which can also be stabilized in YMn_2 by applying pressure, giant spin fluctuations were observed down to very low temperatures [25–27]. For the (Y, Sc)Mn_2 compounds they were analysed by taking account of the anharmonicity of the spin-fluctuation spectrum [28]. Spin fluctuations were found to strongly influence the thermal expansion and transport properties of YMn_2 and YMn_2-based compounds [29, 30]. The quantum spin-liquid state of $Y_{0.97}Sc_{0.03}Mn_2$ considered in [31] should also be referred to the NTP phase.

Some properties of the TP and NTP states, particularly those related to phase coexistence, were studied in detail in the $Y_{1-x}Tb_xMn_2$ [17, 32], $Y_{1-x}Dy_xMn_2$ [20] and $Y_{1-x}Ho_xMn_2$ [33] systems. It was shown that long-range order can be absent also in the TP state; only a short-range ordering was observed in the Mn sublattice of $Tb_{0.4}Y_{0.6}Mn_2$ by means of neutron diffraction either at ambient pressure or at 3 kbar.

In this work the magnetic properties of the $Y_{1-x}Gd_xMn_2$ system are reported. The aim of the study is to ascertain the regularities in the variation of the TP state characteristics as functions of the Gd concentration and external pressure. The lattice parameter changes very little in this system, from 7.680 Å in YMn_2 to 7.750 Å in $GdMn_2$, and its influence on the magnetic properties is expected to be minimal. At the same time, the variation of the f–d exchange interaction in this system is the largest among those of the (Y, R)Mn_2 pseudobinary compounds. Note that the Néel/Curie temperatures are almost equal for both of the two mother compounds YMn_2 and $GdMn_2$, $\sim$100 K and 108 K, respectively, as are the Mn magnetic moments, 2.7 μ_B. In contrast to YMn_2, which has an antiferromagnetic ground state, $GdMn_2$ exhibits antiferromagnetic order down to about 35 K only, below which a spontaneous magnetization appears. The low-temperature magnetic state of $GdMn_2$ was concluded to be ferrimagnetic [5, 14]. It is also worth mentioning some prominent differences between their characteristics, mainly related to the TP state of the Mn sublattice:

(a) the magnetovolume effect in YMn_2 (6%) is considerably larger than those in other RMn_2 compounds (2% in $GdMn_2$);
(b) in YMn_2 the first-order phase transition occurs with much larger hysteresis ($\sim$30 K) than for other RMn_2 compounds ($\leqslant$5 K).

2. Experimental details

Polycrystalline samples of the $Y_{1-x}Gd_xMn_2$ compounds were prepared from starting materials using induction high-frequency melting under a protective argon-gas atmosphere in a water-cooled copper crucible. In order to avoid the formation of the R_6Mn_{23} phase, a stoichiometry of 1:1.93 was chosen. The ingots were subsequently homogenized at 730 °C for five days under a dynamic vacuum in Ta containers. The phase purity of the samples was checked by x-ray diffraction analysis (it was within 2% accuracy). Additionally, the sample purity for the magnetic measurements was controlled by the thermomagnetic method: the content of the high-temperature magnetic phases was determined as $\leqslant$0.2 mol%.

The magnetization up to 50 kOe and the DC susceptibility (in fields up to 10 kOe) were measured over the temperature range 1.8–150 K by a SQUID magnetometer, MPMS-5. For the compounds exhibiting a spontaneous magnetization, a constant field of 2 kOe was used in the $\chi(T)$ measurements. The measurements under pressure were performed by using a pressure cell made from TiCu alloy, which is described elsewhere [34]. The temperature variation of

the pressure in the cell was neglected (within the region 3–7 kbar it was below $\simeq$0.3 kbar [35]). The thermal expansion was measured in the temperature range 5–300 K by the x-ray diffraction method using an Oxford Instruments continuous-flow cryostat CF-100.

3. Experimental results

3.1. The magnetic (x–T) phase diagram

In figure 1 the temperature dependence of the DC magnetic susceptibility is given for some typical $Y_{1-x}Gd_xMn_2$ compounds. The magnetic phase transitions can clearly be detected from the abrupt change of χ for all of the compounds studied. The hysteresis of the magnetic phase transition is rather narrow ($\sim$5 K) in the range $0.3 \leqslant x \leqslant 1.0$ and broadens considerably for $x \leqslant 0.2$. Below T_C on the Gd-rich side ($x \geqslant 0.8$), the susceptibility increases substantially with decreasing temperature and this is followed by the appearance of a spontaneous magnetization.

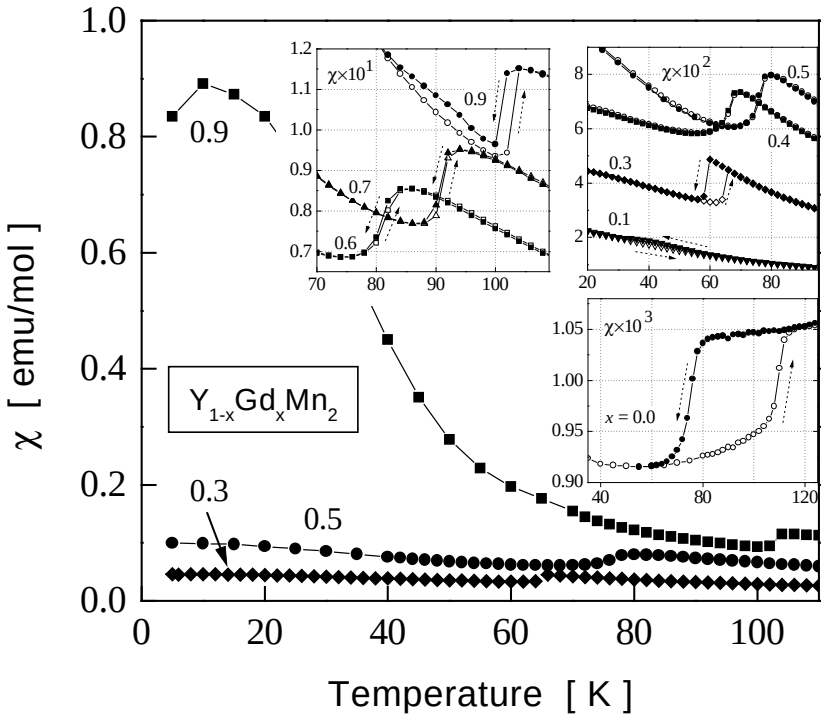

Figure 1. The temperature dependences of the DC susceptibilities of some characteristic $Y_{1-x}Gd_xMn_2$ compounds. The insets show the details in the vicinity of the phase transition.

The temperature dependence of the lattice parameter of this system is shown in figure 2. As can be seen, all of the magnetic transitions are of a first-order type and are accompanied by a large volume expansion of the order of 10^{-2}. The magnetovolume effect occurs for all of the compounds of this system, indicating that the Mn sublattice is ordered (in the TP state) for any Gd content.

The magnetic (x–T) phase diagram of the $Y_{1-x}Gd_xMn_2$ system was constructed using both x-ray thermal expansion and magnetic susceptibility data. It is presented in figure 3. Some disagreement between the thermal expansion and susceptibility data can be attributed

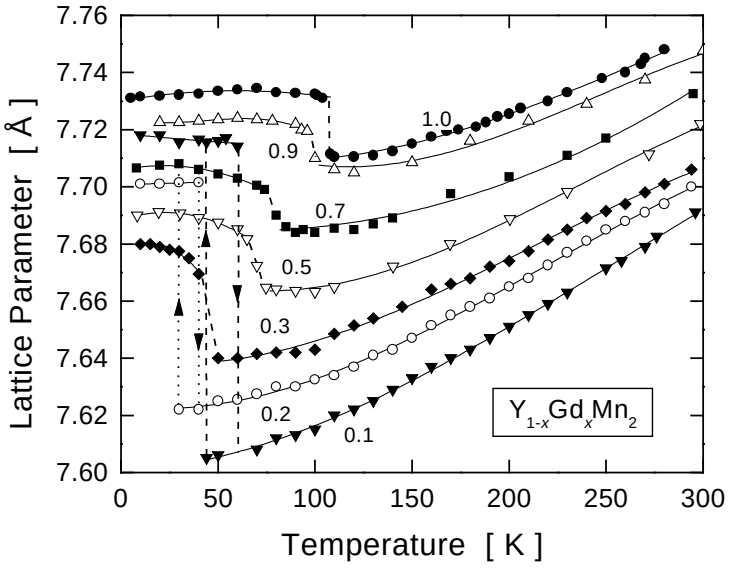

Figure 2. The temperature dependence of the lattice parameter of the $Y_{1-x}Gd_xMn_2$ system. The dashed lines for $x = 0.1$ and 0.2 indicate the region where the paramagnetic and antiferromagnetic phases coexist.

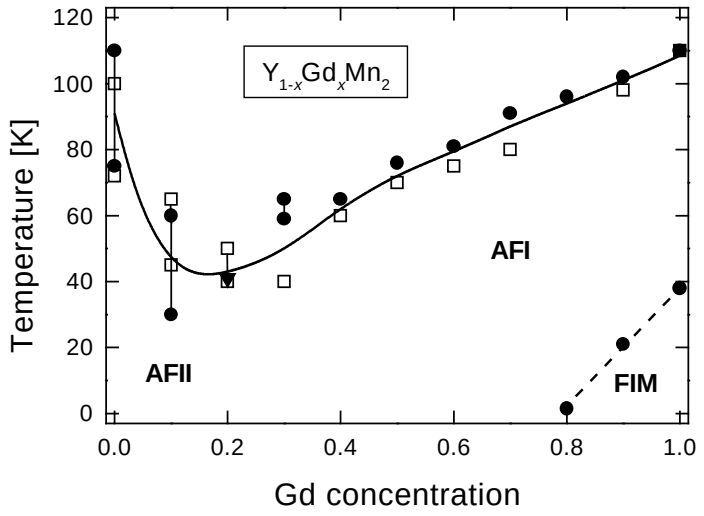

Figure 3. The magnetic (x–T) phase diagram of the $Y_{1-x}Gd_xMn_2$ system. Full circles and open squares indicate the data obtained from the susceptibility and thermal expansion measurements, respectively. For $x \leqslant 0.3$, the vertical lines show the hysteresis range (observed in the $\chi(T)$ measurements) and the region where the AF and paramagnetic phases coexist (according to the x-ray data). The full triangle corresponds to the high-temperature kink of $\chi(T)$ identified as T_N for $Y_{0.8}Gd_{0.2}Mn_2$ (see figure 7, later). AFI and AFII denote the different antiferromagnetic regions; FIM denotes the ferrimagnetic region where a spontaneous magnetization is observed.

to the high sensitivity of T_C/T_N to small variations of the initial stoichiometry (samples from different melts were used in the experiments), a fact repeatedly mentioned previously for RMn_2 compounds [13]. The diagram is characterized by a pronounced minimum at $x = 0.2$. This

concentration separates the compounds with broad ($x \leqslant 0.2$) and narrow ($x \geqslant 0.3$) hystereses observed in $\chi(T)$ and in $a(T)$ dependencies.

3.2. Magnetization measurements

The magnetization curves of the $Y_{1-x}Gd_xMn_2$ compounds at 4 K are given in figure 4. The compounds with $x = 0.8$, 0.9 and 1.0 exhibit a spontaneous magnetization at this temperature. A smooth field-induced phase transition is observed in the concentration range $0.3 \leqslant x \leqslant 0.7$

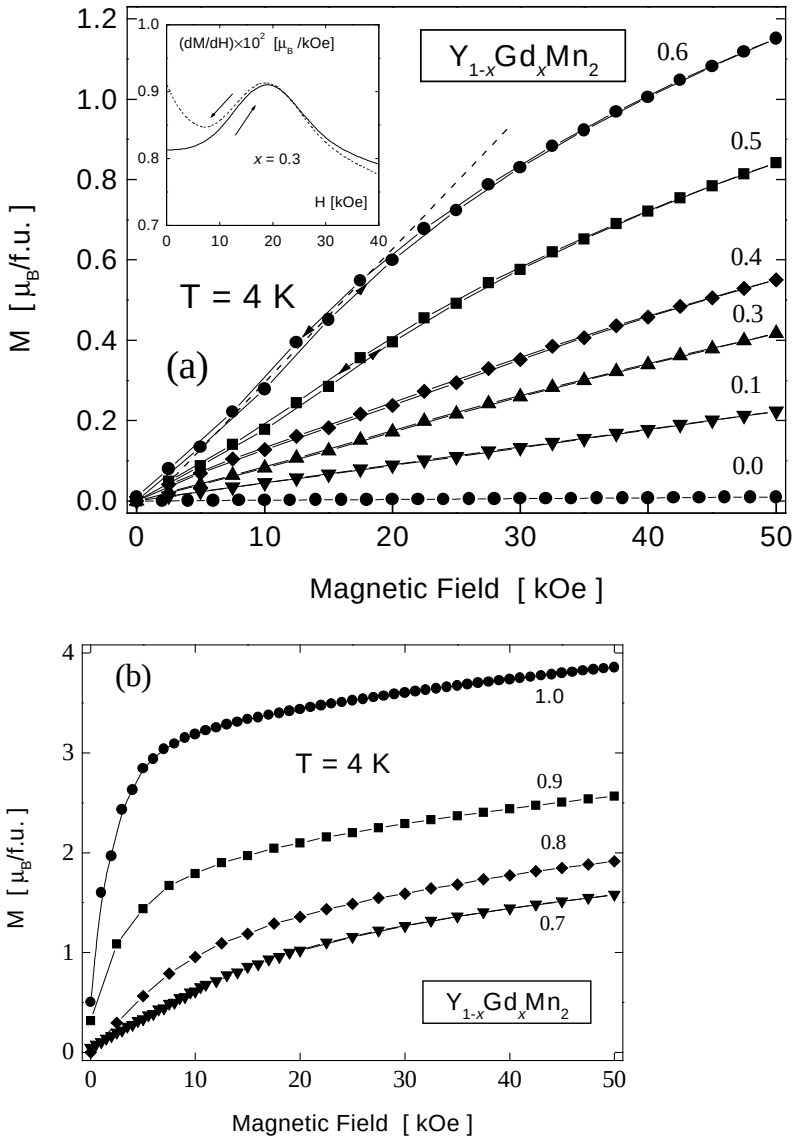

Figure 4. Magnetization curves of the $Y_{1-x}Gd_xMn_2$ compounds at 4 K for low (a) and high (b) Gd concentrations. The dashed line is drawn through $M(H)$ for $Y_{0.4}Gd_{0.6}Mn_2$ in order to highlight the critical field H_C. Arrows indicate the field hysteresis. The field variation of dM/dH for one sample, $Y_{0.7}Gd_{0.3}Mn_2$, is displayed in the inset.

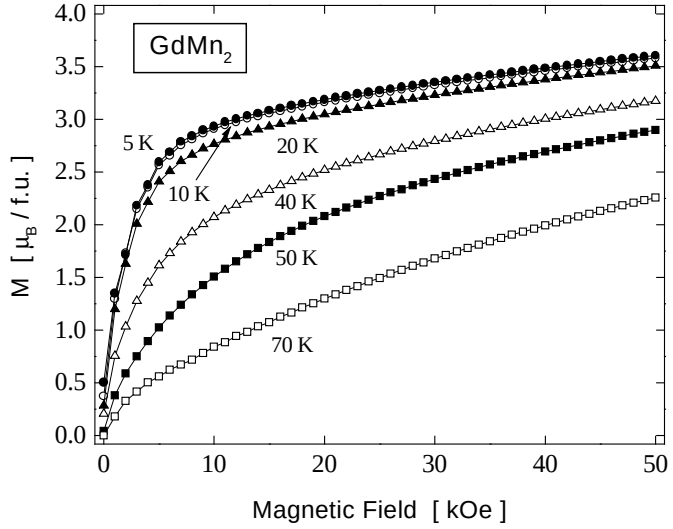

Figure 5. Magnetization curves of $GdMn_2$ at different temperatures.

which can be disclosed by differentiation with respect to H. The critical field of the transition tends to zero near $x = 0.8$.

In figure 5 the magnetization curves of $GdMn_2$ at different temperatures are shown. As can be seen, the spontaneous magnetic moment, M_S, disappears near 40 K. In the region below 40 K any hysteresis phenomena are terminated above 8 kOe. The magnetization curves of $Y_{0.1}Gd_{0.9}Mn_2$ are similar, and M_S reduces to zero at 20 K.

The temperature change of $M(H)$ of a typical AF compound, $Y_{0.5}Gd_{0.5}Mn_2$ ($T_N = 76$ K), of this system is shown in figure 6(a). The values of H_C are weakly dependent on temperature, the transition being observable up to 70 K (figure 6(b)). Similar behaviour is exhibited by the other antiferromagnetic compounds for the interval $0.3 \leqslant x \leqslant 0.7$, too.

The $Y_{0.8}Gd_{0.2}Mn_2$ compound is very distinctive. Although a clear abrupt jump with a hysteresis of about 10 K is observed in the temperature dependence of the lattice parameter, the DC susceptibility does not show any jump or hysteresis which might be associated with the first-order phase transition. At 41 K, which was identified as the transition point, the susceptibility shows a characteristic kink. A freezing effect arises below $T_f = 30$ K. As can be seen from figure 7, the variation of χ versus T for the zero-field-cooled (z.f.c.) sample differs markedly from that measured when cooling under 50 kOe.

Figure 8 shows the magnetization cycling of $Y_{0.8}Gd_{0.2}Mn_2$ at 4 K measured under different conditions. The magnetization process over the whole field range from -50 to 50 kOe is accompanied by an extended hysteresis. The magnetization curve of the 50 kOe field-cooled (f.c.) sample is irreversible and becomes nearer to the z.f.c. curve after cycling. Over the temperature interval 30–41 K the sample does not show either irreversibility or a spontaneous magnetization, and is probably in the antiferromagnetic state. The fact that the z.f.c. magnetization process runs outside the hysteresis loop of the f.c. cycle indicates that the magnetic structures of the f.c. and z.f.c. states are different. This behaviour resembles a re-entrant freezing phenomenon with the sequence paramagnetism $\rightarrow$ antiferromagnetism $\rightarrow$ frozen magnetic phase on cooling. The magnetization signal of $Y_{0.8}Gd_{0.2}Mn_2$ is time

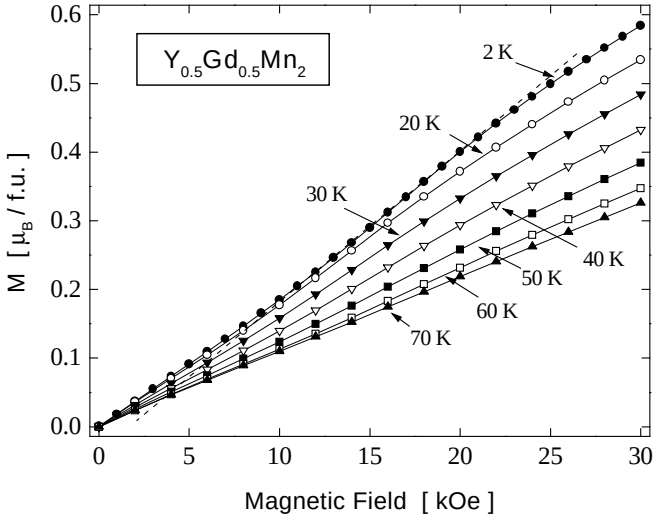

(a)

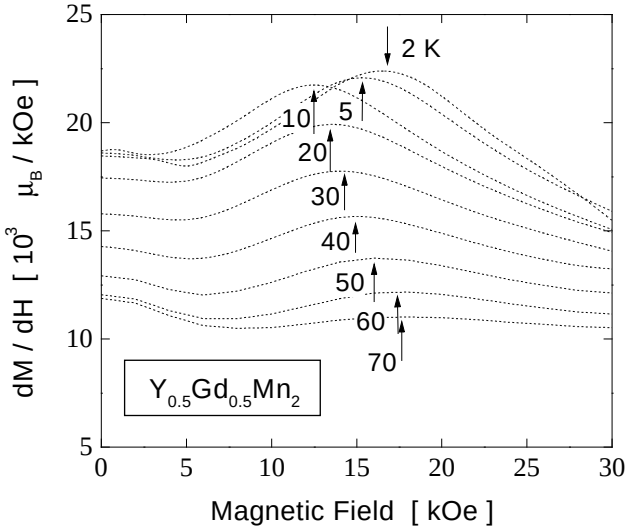

(b)

Figure 6. Magnetization curves of $Y_{0.5}Gd_{0.5}Mn_2$ (a) and the variation of the derivatives dM/dH as functions of the magnetic field (b) at different temperatures. The dashed line is drawn through $M(H)$ at 2 K in order to highlight the critical field H_C. Arrows in (b) indicate the positions of H_C.

dependent below 20 K. The $M(t)$ curves can be well approximated by the expression

$$M(t) = M_\infty + \Delta M_1 \, e^{-t/\tau_1} + \Delta M_2 \, e^{-t/\tau_2} \tag{1}$$

which points to the presence of two relaxation mechanisms. At 4.5 K, the following values were found for the relaxation times of the magnetization signal at 5 kOe of a sample cooled under 50 kOe: $\tau_1 = 10$ min and $\tau_2 = 115$ min.

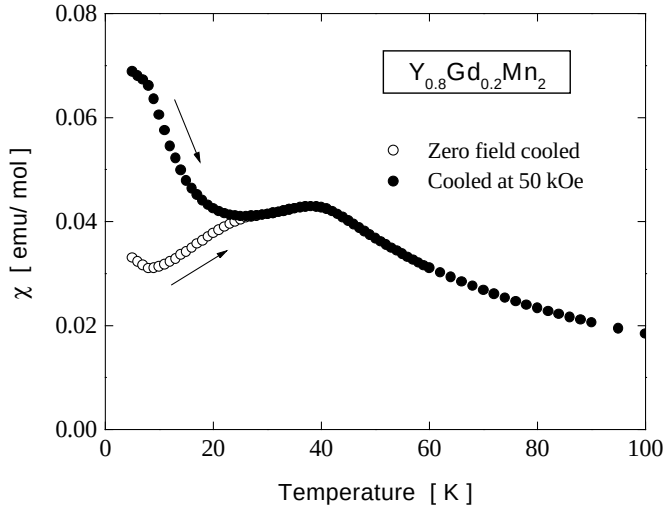

Figure 7. The DC susceptibility of $Y_{0.8}Gd_{0.2}Mn_2$ as a function of temperature measured on heating for the sample cooled down in zero field and under 50 kOe.

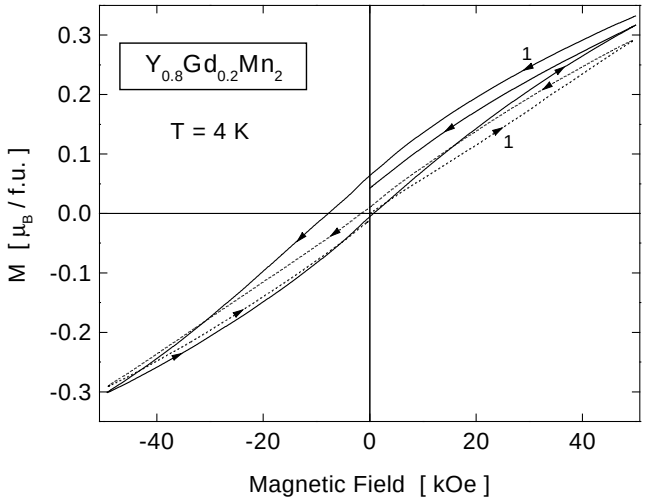

Figure 8. The magnetization process of $Y_{0.8}Gd_{0.2}Mn_2$ at 4 K. The dotted curve corresponds to the z.f.c. initial state and the solid curve is for the sample cooled down under 50 kOe. For both curves, the first magnetization trace is indicated by the digit 1.

3.3. Magnetic properties of the $Y_{1-x}Gd_xMn_2$ compounds under pressure

The effect of pressure on the magnetization process of $Y_{0.7}Gd_{0.3}Mn_2$ is shown in figure 9. The magnetization curves for the z.f.c. and f.c. samples are slightly different at ambient pressure. The f.c. sample shows a narrow hysteresis, the field-induced magnetic phase transition still being detectable by differentiating at $\simeq$19 kOe. Under external pressure the following characteristic properties appear:

(a) The magnetization curve of the z.f.c. cycle has a negative curvature with a narrow hysteresis. No field-induced transition can be detected at 5 kbar. At the same time, the

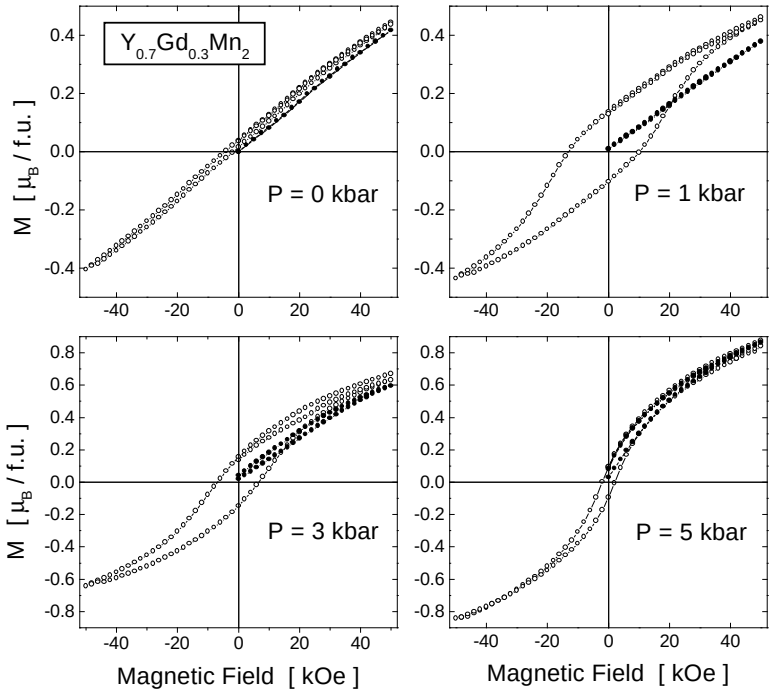

Figure 9. The hysteresis loops of $Y_{0.7}Gd_{0.3}Mn_2$ at 4 K under different pressures. Full and open symbols correspond to the z.f.c. and f.c. (50 kOe) sample, respectively.

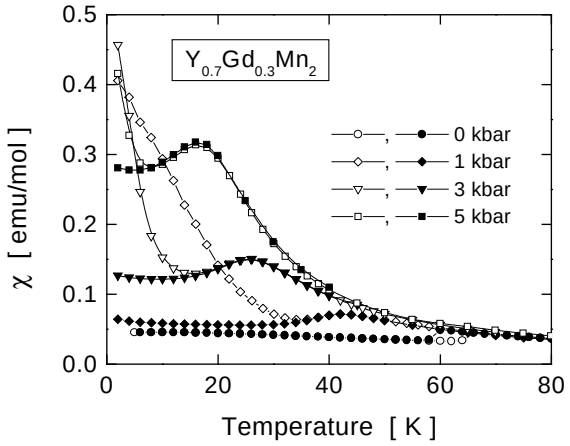

Figure 10. The DC susceptibility of $Y_{0.7}Gd_{0.3}Mn_2$ as a function of temperature under different pressures measured on heating for the sample cooled down at zero field (full symbols) and 50 kOe (open symbols).

high-field magnetization value increases substantially (at 50 kOe, from 0.41 μ_B/f.u. to 0.82 μ_B/f.u.).

(b) The magnetization curve of the f.c. cycle shows a wide hysteresis under pressure. The hysteresis width is maximal at 1 kbar. A clear irreversibility of the $M(H)$ curve appears at 3 kbar, which is the consequence of a slow relaxation.

This is similar to what was observed for the $Y_{0.8}Gd_{0.2}Mn_2$ at ambient pressure. With the further increase of pressure the hysteresis loop becomes narrower and the $M(H)$ curves for the z.f.c. and f.c. cycles almost coincide. The magnetization curves for the z.f.c. sample at $P = 1$ kbar and 3 kbar lie outside the hysteresis loop of the f.c. sample.

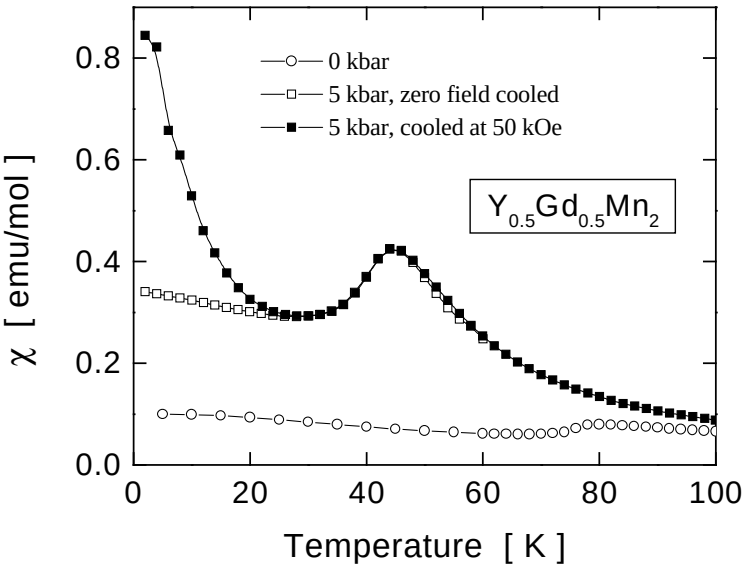

Figure 11. The DC susceptibility of $Y_{0.5}Gd_{0.5}Mn_2$ as a function of temperature measured at ambient pressure and under 5 kbar.

Figure 10 displays the appearance of the freezing effect in $Y_{0.7}Gd_{0.3}Mn_2$ induced by pressure. Under low pressure the temperature dependence of $\chi(T)$ can be transformed into that observed for $Y_{0.8}Gd_{0.2}Mn_2$ at $P = 0$. A similar, however less prominent, change in $\chi(T)$ also occurs for the compounds with higher Gd concentration. In figure 11 the temperature dependencies of the magnetic susceptibility of $Y_{0.5}Gd_{0.5}Mn_2$ at $P = 0$ and 5 kbar are compared. Application of external pressure results in the appearance of a small remnant magnetization in the f.c. sample; at 5 kbar it arises below $T_f = 22$ K. As in the case of $Y_{0.7}Gd_{0.3}Mn_2$, a substantial increase of M occurs (see figure 12). The magnetization at 50 kOe rises from 0.82 μ_B/f.u. (0 kbar) to 1.22 μ_B/f.u. (5 kbar). In this compound the z.f.c. magnetic structure is antiferromagnetic with the field-induced magnetic phase transition still persisting under pressure up to 5 kbar. The sample shows, however, some magnetic inhomogeneity below T_f, which can be detected by cycling: the transition smears and a small hysteresis can be seen when demagnetizing (figure 13). Again, the magnetization processes for the 50 kOe f.c. and z.f.c. samples differ substantially, the former occurring with much broader hysteresis and a higher value of the magnetization. The inset in figure 12 shows that the field-induced magnetic phase transition shifts to the lower-field region under pressure.

4. Discussion

The magnetic phase diagram presented in figure 3 shows that most of the structures realized in the $Y_{1-x}Gd_xMn_2$ system are antiferromagnetic. A non-compensated ferrimagnetic structure exists, but only in the low-temperature region of the Gd-rich side with $x \geqslant 0.8$. Note that at

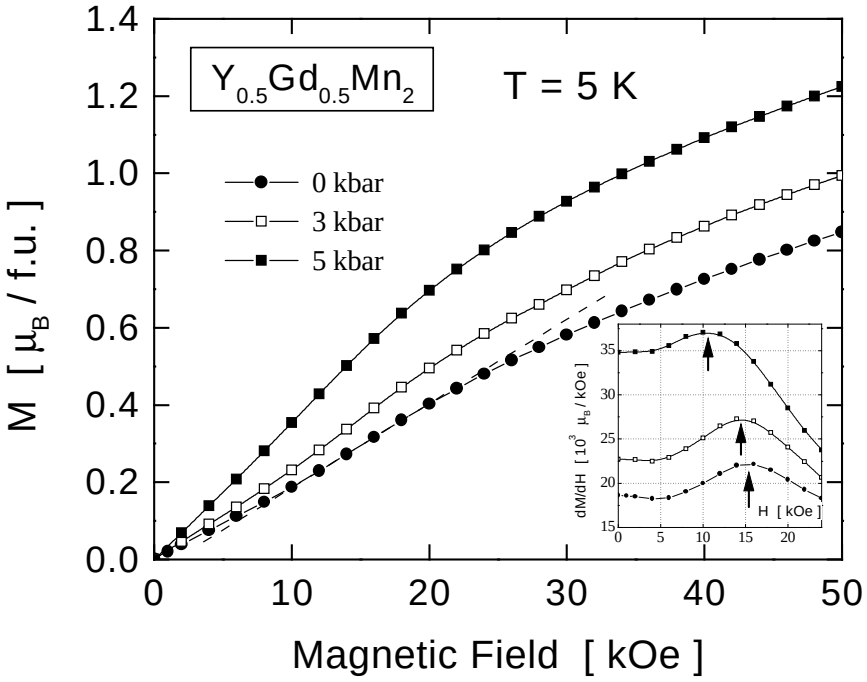

Figure 12. Magnetization curves of $Y_{0.5}Gd_{0.5}Mn_2$ at 5 K measured under different pressures. The dashed line is drawn through $M(H)$ at 0 kbar in order to highlight the critical field H_C. The inset shows the variation of the derivatives dM/dH as functions of the magnetic field. The arrows in the inset indicate the positions of H_C.

$T \to 0$ the boundary between the AF and FIM phases corresponds to the magnetic compensation of a collinear ferrimagnetic arrangement of the Mn and Gd magnetic moments. Taking $\mu_{\mathrm{Mn}} = 2.7\ \mu_{\mathrm{B}}$ and $\mu_{\mathrm{Gd}} = 7.0\ \mu_{\mathrm{B}}$, the magnetic compensation occurs at $x_{comp} = 0.77$. At present we cannot explicitly relate this value to the magnetic structure of the $Y_{1-x}Gd_xMn_2$ compounds. Another characteristic boundary concentration can be distinguished at the concentration $x = 0.2$, above which the hysteresis accompanying the first-order-type transition shrinks abruptly and field-induced magnetic phase transitions can be observed. Although the different magnetic structures distinguished in the $Y_{1-x}Gd_xMn_2$ system cannot be solved by macroscopic measurements, some conclusions can be deduced from the above experiments.

The high-field magnetization of the Gd-rich ferrimagnetic compounds is substantially smaller than the value expected for a saturated Gd sublattice. For $TbMn_2$, the antiparallel alignment of the resulting Mn- and Tb-sublattice magnetizations was proved by magnetization and magnetostriction measurements [11, 14]. Hence, the f–d exchange interaction dominates in this compound over the f–f and d–d ones. The same holds for $GdMn_2$, too, as the Gd–Mn interaction can be considered stronger than the Tb–Mn one. In $GdMn_2$, the d–d interaction also seems stronger than that in $TbMn_2$ as at higher temperatures the antiferromagnetic state becomes stable. The fact that the ferrimagnetic phase disappears at $x < x_{comp}$ indicates that in the $Y_{1-x}Gd_xMn_2$ system the d–d and f–d interactions are of the same order of magnitude. This could be due to the larger lattice parameter of $GdMn_2$, which makes the Mn magnetism more stable than in $TbMn_2$.

Consider now the AF compounds with x in the concentration interval $0.3 \leqslant x \leqslant 0.7$, which exhibit a field-induced magnetic phase transition. The magnetization measurements

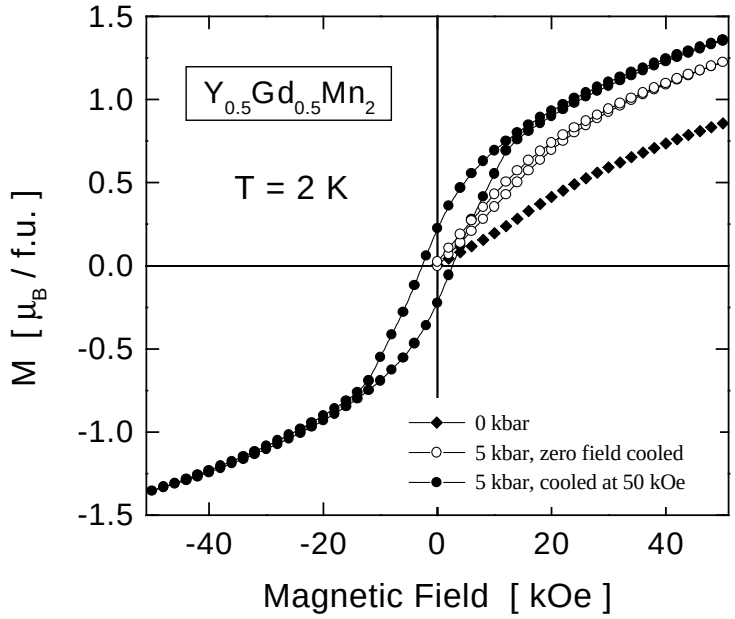

Figure 13. The magnetization process of $Y_{0.5}Gd_{0.5}Mn_2$ under different pressures.

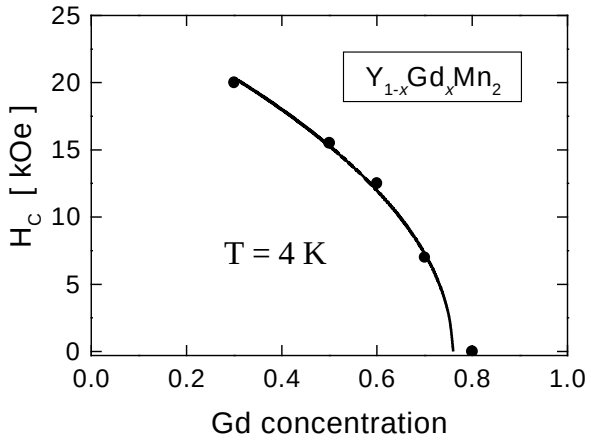

Figure 14. The low-temperature concentration dependence of the critical field H_C for the $Y_{1-x}Gd_xMn_2$ system. The solid curve was drawn using the least-squares fit according to equations (2) and (3).

do not allow us to establish the exact spin arrangement of these compounds. However, some general conclusions can be reached proceeding from the concentration dependence of H_C, the critical field of the transition. As figure 14 shows, H_C drops with increasing Gd concentration and reduces to zero near x_{comp}.

The antiferromagnetic spin arrangement in this range (AFI) can be treated as formed by separate Gd and Mn antiferromagnetic sublattices (weak f–d exchange); alternatively it can be considered as made up of antiparallel coupled Gd–Mn moments, which form an antiferromagnetic structure owing to the negative d–d exchange interaction (strong f–d

exchange). The difference between the two approaches depends on the relative strength of the d–d, f–d and f–f interactions, and becomes important under an external field. In the antiferromagnetic state, the net magnetization under the magnetic field $\boldsymbol{H}$ can be expressed in the form

$$M_{net} = M_{\mathrm{Mn}}(H) + M_{\mathrm{Gd}}(H) = 2\mu_{\mathrm{Mn}}\frac{1}{L}\sum_{i=1}^{L}\cos\vartheta_i + x\mu_{\mathrm{Gd}}\frac{1}{N}\sum_{j=1}^{N}\cos\vartheta_j \qquad (2)$$

where $\vartheta_i(H)$ and $\vartheta_j(H)$ are the angles between $\boldsymbol{H}$ and the magnetic moments of Mn and Gd in the i- and j-sublattices, respectively, L and N being the numbers of the sublattices. In the $x < 0.77$ range M_{Mn} is larger than M_{Gd}; therefore the Mn moments tend to be aligned along the applied field (as ϑ_i vary from 90° to 0°, $\cos\vartheta_i$ is always positive). Hence, the observed transition at H_C cannot be associated with the reverse magnetization process occurring in the Mn sublattice due to the magnetic instability. It follows from the magnetization curves of $GdMn_2$ ($H_a < 10$ kOe) that the magnetic anisotropy must be small in these compounds. Therefore a smearing over the field interval 15 kOe indicates that it is a second-order-type phase transition, which can be related to a rearrangement of the magnetic structure due to a spin-flopping process. We therefore relate it to a spin-flop-type transition, which only changes the orientation and does not change the magnitude of the magnetic moments.

In contrast, $\cos\vartheta_j$ can be either positive (weak f–d interaction) or negative (strong f–d interaction). In the latter case, the Gd and Mn moments move in opposite directions under a field. Thus, depending on the strength of the f–d interaction, M_{net} must either increase (weak f–d interaction) or decrease (strong f–d interaction) with increasing Gd concentration. For a qualitative analysis, the conventional expression for the spin-flop transition field of weakly anisotropic antiferromagnets can be used:

$$H_C = \sqrt{\lambda H_A M_{net}} \qquad (3)$$

where λ is the intersublattice molecular-field coefficient and H_A is the anisotropy field, M_{net} being the net field-induced magnetization per f.u. (sublattice magnetization) at $H = H_C$. As seen from equation (3), for the weak f–d exchange H_C must increase with increasing Gd concentration, which is inconsistent with the experiment. In contrast, the latter suggested hierarchy is in agreement with the experimental variation of $H_C(x)$.

The least-squares fit of equation (3) to the experimental $H_C(x)$ dependence performed with the fixed values $\mu_{\mathrm{Gd}} = 7.0\ \mu_{\mathrm{B}}$ and $\mu_{\mathrm{Mn}} = 2.7\ \mu_{\mathrm{B}}$ has given

$$L\lambda H_A \Big/ \sum_i \cos\vartheta_i = 127\ \mathrm{kOe}^2/\mu_{\mathrm{B}}$$

and

$$L\sum_j \cos\vartheta_j \Big/ N\sum_i \cos\vartheta_i = -1 \pm 0.02$$

(here the concentration dependencies of the f–d interaction strength and anisotropy field are neglected). As seen from figure 14, the calculated $H_C(x)$ dependence agrees well with the experimental data. This result shows that μ_{Gd} and μ_{Mn} remain antiparallel to each other in an external magnetic field, and the antiferromagnetic structure in this concentration range can be treated as being formed by equivalent magnetic sublattices with the sublattice magnetization taken as $M_{net} = 2\mu_{\mathrm{Mn}} - x\mu_{\mathrm{Gd}}$.

In order to discuss the phase diagram of the $Y_{1-x}Gd_xMn_2$ system for the low-Gd-concentration region, $x \leqslant 0.2$, consider the concentration dependencies of the pressure response of T_N and the volume expansion accompanying the magnetic phase transition, $\omega_S = (V_m - V_0)/V_0$ (V_m and V_0 being the volumes of the elementary cell below and

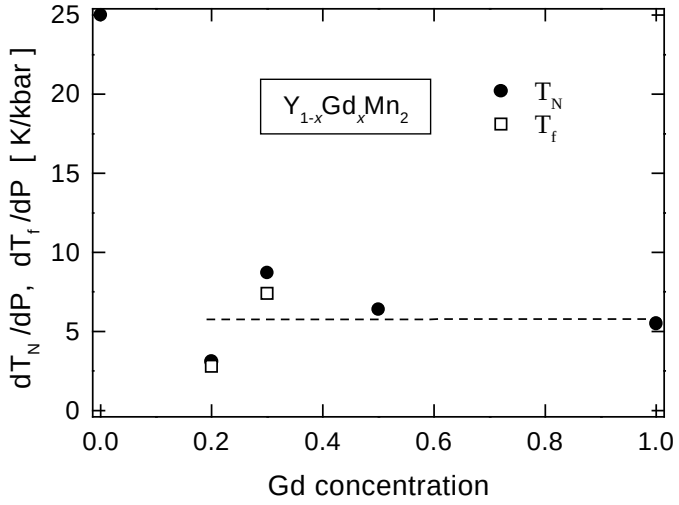

Figure 15. The concentration dependences of $\mathrm{d}T_N/\mathrm{d}P$ and $\mathrm{d}T_f/\mathrm{d}P$ for the $Y_{1-x}Gd_xMn_2$ system. The dashed straight line in the figure is drawn as a guide to the eye in the region $x > 0.2$.

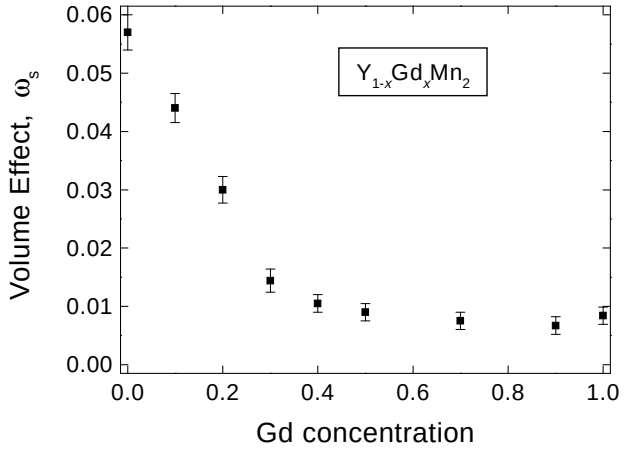

Figure 16. The concentration dependence of the volume effect, ω_S, for the $Y_{1-x}Gd_xMn_2$ system.

above the transition point, respectively), shown in figures 15 and 16. Both, $\partial T_N/\partial P$ and ω_S show substantial increase below $x = 0.2$. In this concentration region, the Gd sublattice is disordered (see for comparison other $Y_{1-x}Gd_xMe_2$ systems [36]), and the antiferromagnetic AFII magnetic structure can be considered as determined mainly by the d–d exchange interaction as in the mother compound YMn_2. Then the decrease of T_N at low Gd content, which results in there being a minimum at $x \approx 0.2$, is a consequence of the growing magnetic instability induced by the Gd–Mn negative exchange interaction. This interaction upsets the exchange balance of the fully frustrated YMn_2-like AFII structure. In contrast, the AFI-type magnetic structure of the Gd-rich compounds is mainly stabilized by the f–d exchange interaction. Therefore the differences in the values of $\partial T_N/\partial P$ and ω_S can be related to the different factors responsible for the stability of the AFI and AFII structures.

$Y_{0.8}Gd_{0.2}Mn_2$ is an intermediate compound in the phase diagram. This compound,

although being in the TP state, has characteristics of short-range order below 30 K. The first anomaly, both in $a(T)$ and $\chi(T)$, appears, however, at the considerably higher temperature of 41 K. It is likely that the magnetic state of $Y_{0.8}Gd_{0.2}Mn_2$ passes through the sequence paramagnetism $\rightarrow$ antiferromagnetism $\rightarrow$ short-range order on cooling. The antiferromagnetic state between 30 K and 41 K is of the AFII type, as no field-induced magnetic transitions were observed for that compound around the expected value of $H_C \approx 25$ kOe. It is questionable to relate the short-range order to a 'classical' spin-glass behaviour just on the basis of the magnetization measurements, since both of the relaxation processes found in $Y_{0.8}Gd_{0.2}Mn_2$ are essentially rapid. The nature of the short-range order in $Y_{0.8}Gd_{0.2}Mn_2$ is not yet clear. It could be ascribable to a re-entrant transformation from the TP to NTP state (hence characterizing the transformation rate), or it could be caused by the competition between the AFI and AFII structures, i.e. have a magnetic origin.

The magnetic phase diagrams of the $Y_{1-x}Tb_xMn_2$ (TP state [17]) and $Y_{1-x}Gd_xMn_2$ systems are qualitatively similar. In the former system, $Y_{0.6}Tb_{0.4}Mn_2$ in the TP state showed only short-range correlations at low temperatures, similarly to what was observed for $Y_{0.8}Gd_{0.2}Mn_2$. The region of short-range correlations first broadens with increasing pressure; under 1 kbar it is extended up to at least $x = 0.3$. Then T_f, like T_N, shifts towards lower temperatures with further increasing pressure. Pressure up to 5 kbar is still not enough to cause the NTP state to arise in the $Y_{1-x}Gd_xMn_2$ system.

The application of external pressure results in a considerable increase of the net magnetization in the AFI state (see figures 9, 12 and 13) and leads also to the increase of H_C. The behaviour of M versus P cannot be directly associated with the instability of the Mn magnetism, i.e. with the pressure-induced TP $\rightarrow$ NTP transition. In this concentration region ($M_{\mathrm{Mn}} > M_{\mathrm{Gd}}$) the magnetic field aligns the Mn moments; hence the change of μ_{Mn} from 2.7 μ_{B} to 1.4 μ_{B} would lead to a decrease of the magnetization value under a field. Considering the Mn sublattice to be still in the TP state at low pressure, the increase of $M(H)$ and H_C can be understood as a breaking down of the antiparallel Gd–Mn coupling by pressure. Then, according to equation (3), an increase of H_C is also expected.

5. Conclusions

The magnetic properties of the RMn_2 compounds can be interpreted by suggesting that the first-order phase transition related to the onset of antiferromagnetic order in the Mn sublattice has a non-magnetic origin, being a kind of structural transformation. In the $Y_{1-x}Gd_xMn_2$ system the transformed phase with a strongly expanded lattice is stable at any Gd concentration.

At least two magnetic structures of antiferromagnetic type can be distinguished in the $Y_{1-x}Gd_xMn_2$ system, YMn_2-type and $GdMn_2$-type structures. In the latter structure the antiparallel alignment of the Gd and Mn moments is proved by the observation of field-induced magnetic phase transitions. The $GdMn_2$-type antiferromagnetic structure is, nevertheless, non-collinear and can be considered as formed by the net magnetization vector $M_{net} = 2\mu_{\mathrm{Mn}} - x\mu_{\mathrm{Gd}}$. Above the compensation point $x_{comp} = 0.77$ the Gd sublattice is also ordered antiferromagnetically; this conclusion applies to the temperature interval 40 K–T_N for $GdMn_2$, too.

The intermediate compound $Y_{0.8}Gd_{0.2}Mn_2$ shows characteristics of short-range order in the transformed phase. This compound resembles $Y_{0.6}Tb_{0.4}Mn_2$, for which the absence of long-range order was proved by neutron diffraction. External pressure up to 5 kbar is not enough to suppress the transformed phase completely; however, the magnetic structure of the $Y_{1-x}Gd_xMn_2$ compounds in the transformed phase is strongly modified by pressure.

Acknowledgments

This work was supported by a Grant-in-Aid for Scientific Research on Priority Areas (Nos 09740535 and 09217253) from the Ministry of Education, Science and Culture, Japan, and Nissan Foundation of Science. We also acknowledge the financial support obtained from RFBR (Project 96-02-16846) and INTAS (Project 96-0630).

We thank the Japan Society for the Promotion of Science (JSPS) for the Special Researcher Fellowship given to ASM.

References

[1] Levitin R Z and Markosyan A S 1988 *Sov. Phys.–Usp.* **31** 730
[2] Wada H, Nakamura H, Yoshimura K, Shiga M and Nakamura Y 1987 *J. Magn. Magn. Mater.* **70** 134
[3] Nakamura Y, Shiga M and Kawano S 1983 *Physica* B **129** 212
[4] Yoshimura K and Nakamura Y 1984 *J. Phys. Soc. Japan* **53** 3611
[5] Gaidukova I Yu, Kruglyashov S B, Markosyan A S, Levitin R Z, Pastushenkov Yu G and Snegirev V V 1983 *Sov. Phys.–JETP* **57** 1083
[6] Ritter C, Kilcoyne S H and Cywinski R 1991 *J. Phys.: Condens. Matter* **3** 727
[7] Ballou R, Deportes J, Lemaire R, Nakamura Y and Ouladdiaf B 1987 *J. Magn. Magn. Mater.* **70** 129
[8] Brown P J, Ouladdiaf B, Ballou R, Deportes J and Markosyan A S 1992 *J. Phys.: Condens. Matter* **4** 1103
[9] Yoshimura K and Nakamura Y 1984 *J. Magn. Magn. Mater.* **40** 55
[10] Shiga M 1988 *Physica* B **149** 293
[11] Gaidukova I Yu, Dubenko I S and Markosyan A S 1985 *Phys. Met. Metallogr.* **59** 79
[12] Gratz E, Lindbaum A, Markosyan A S, Mueller H and Sokolov A Yu 1994 *J. Phys.: Condens. Matter* **4** 6699
[13] Gaidukova I Yu, Dubenko I S, Levitin R Z, Markosyan A S and Pirogov A N 1988 *Sov. Phys.–JETP* **67** 2522
[14] Ibarra M R, Marquina C, Garcia-Orza L, Arnold Z and del Moral A 1994 *J. Appl. Phys.* **75** 5662
[15] Ibarra M R, Arnold Z, Marquina C, Garcia-Orza L and del Moral A 1994 *J. Appl. Phys.* **75** 7158
[16] Ibarra M R, Marquina C, Garcia-Orza L, Arnold Z and del Moral A 1993 *J. Magn. Magn. Mater.* **128** L249
[17] De Teresa J M, Ritter C, Ibarra M R, Arnold Z, Marquina C and del Moral A 1996 *J. Phys.: Condens. Matter* **8** 8385
[18] Gaidukova I Yu and Markosyan A S 1982 *Phys. Met. Metallogr.* **54 168**
[19] Nakamura H, Wada H, Yoshimura K, Shiga M and Nakamura Y 1988 *J. Phys. F: Met. Phys.* **18** 981
[20] Ritter C, Cywinski R, Kilcoyne S H, Mondal S and Rainford B D 1994 *Phys. Rev.* B **50** 9894
[21] Oomi G, Terada T, Shiga M and Nakamura Y 1987 *J. Magn. Magn. Mater.* **70** 137
[22] Voiron J, Ballou R, Deportes J, Galera R M and Lelievre E 1991 *J. Appl. Phys.* **69** 5678
[23] Endo S, Tanaka R, Nakamichi S, Ono F, Wada H and Shiga M 1992 *J. Magn. Magn. Mater.* **104–107** 1441
[24] Hauser R, Bauer E, Gratz E, Häufler Th, Hilsher G and Wiesinger G 1994 *Phys. Rev.* B **50** 13 493
[25] Wada H, Nakamura H, Fukami E, Yoshimura K, Shiga M and Nakamura Y 1987 *J. Magn. Magn. Mater.* **70** 17
[26] Freltoft T, Böni P, Shirane G and Motoya K 1988 *Phys. Rev.* B **37** 3454
[27] Block A, Mohsen M, Abd-Elmeguid M and Micklitz H 1994 *Phys. Rev.* B **49** 12 365
[28] Lacroix C, Solontsov A Z and Ballou R 1996 *Phys. Rev.* B **54** 15 178
[29] Shiga M, Wada H, Nakamura H, Yoshimura K and Nakamura Y 1987 *J. Phys.: Met. Phys.* **17** 1781
[30] Hauser R, Bauer E, Gratz E, Dubenko I S and Markosyan A S 1994 *Physica* B **199+200** 662
[31] Shiga M, Fujisawa K and Wada H 1993 *J. Phys. Soc. Japan* **62** 1329
[32] de Teresa J M, Ibarra M R, Ritter C, Marquina C, Arnold Z and del Moral A 1995 *J. Phys.: Condens. Matter* **7** 5643
[33] Ritter C, Cywinski R and Kilcoyne S H 1994 *Z. Naturf.* a **50** 191
[34] Hosokoshi Y, Tamura M and Kinoshita M 1997 *Mol. Cryst. Liq. Cryst.* **306** 423
[35] Hosokoshi Y, Mitoh M, Tamura M, Takeda K, Inoue K and Kinoshita M 1998 *Rev. High Pressure Sci. Technol.* **7** 620
[36] Burzo E 1981 *Bull. Magn. Reson.* **2** 239